INTERNATIONAL JOURNAL FOR NUMERICAL AND ANALYTICAL METHODS IN GEOMECHANICS
Int. J. Numer. Anal. Meth. Geomech. 2010; **34**:978–990
Published online 14 October 2009 in Wiley InterScience (www.interscience.wiley.com). DOI: 10.1002/nag.848

Discrete element modeling of direct shear tests for a granular material

Ying Yan[1] and Shunying Ji[2,*,†]

[1]*Dalian Jiaotong University, School of Civil and Safety Engineering, Dalian 116028, People's Republic of China*
[2]*State Key Laboratory of Structural Analysis for Industrial Equipment, Dalian University of Technology, Dalian 116023, People's Republic of China*

SUMMARY

A succinct 3D discrete element model, with clumps to resemble the real shapes of granular materials, is developed. The quaternion method is introduced to transform the motion and force of a clump between local and global coordinates. The Hertz–Mindlin elastic contact force model, incorporated with the nonlinear normal viscous force and the Mohr–Coulomb friction law, is used to describe the interactions between particles. The proposed discrete element model is used to simulate direct shear tests of the irregular limestone rubbles. The simulation results of vertical displacements and shear stresses with a mixture of clumps are compared well with that of laboratory tests. The bulk friction coefficients are calculated and discussed under different contact friction coefficients and normal stresses. Copyright © 2009 John Wiley & Sons, Ltd.

Received 26 November 2008; Revised 1 September 2009; Accepted 1 September 2009

KEY WORDS: discrete element method; clumps; direct shear test

1. INTRODUCTION

Direct shear tests have been widely used to investigate the shear strength and dilatancy of granular materials such as soil, rock and powder. For the numerical simulations of direct shear tests, finite element method has been adopted together with elastic–plastic or hypoplastic constitutive models with hardening effect [1, 2]. However, based on the continuum constitutive model, it is difficult to take properties of granular materials into account such as particle size, particle shape, void ratio and roughness, which are important parameters in the studies of mechanical behaviors of granular

*Correspondence to: Shunying Ji, State Key Laboratory of Structural Analysis for Industrial Equipment, Dalian University of Technology, Dalian 116023, People's Republic of China.
†E-mail: jisy@dlut.edu.cn

Contract/grant sponsor: National Natural Science Foundation of China; contract/grant numbers: 10772041, 50808027
Contract/grant sponsor: Scientific Research Foundation for the Returned Overseas Scholars, State Education Ministry; contract/grant number: 2008-890

materials. In recent years, discrete element method (DEM) has been used in the simulation of direct shear tests of granular materials and particles have been modeled using 2D disks or 3D spheres [3, 4].

It is easier to model the interactions between regular shaped particles than those of irregular ones. However, granular materials have complex configurations naturally. In order to reasonably describe the particle arrangement and the dynamics of irregular shaped granular materials, analytically defined particle shapes, such as elliptical and super-quadric, have been established accordingly [5, 6]. In addition, clusters formed by bonding or clumps formed by clumping multiple disks or spheres, offer another effective way to model realistic particles [7–11]. Clustered elements, created by bonding regular particles without initial overlap, are allowed to break up under large particle interaction and deformation, and suitable to study crushable materials [7–9]. Clumped particles are generated by clumping disks or spheres with prescribed initial overlap without generating interaction force, and all of clumped particles move as one element that will not break apart [9–11].

Clumping method has been used in the DEM software PFC^{2D} and PFC^{3D} (particle flow code) developed by Itasca, and successfully applied in rock engineering [9]. However, there equations of motion are calculated in the global coordinates. The moments of inertia of clumps need to be updated in the global coordinates at each time step, which results in overelaborate calculating procedures. Because the clump is treated as a rigid body, its motion can be described by the translational motion of a point in the clump and the rotational motion of the entire clump [9]. The quaternion method, as an alternative way to define rotations in 3D, has the advantage of low computational burden and without singularities, and has been widely used in molecular dynamics, quantum mechanics and rigid body dynamics [12]. So, in the proposed discrete element model with clumps, the quaternion method is introduced to calculate the transformation of the rotation, the resultant force and moment acting on a clump between local and global coordinates.

On the other hand, in the DEM simulation of granular materials, the linear viscous–elastic contact model with Mohr–Coulomb friction law has been widely used. In reality, for most granular materials, the nonlinear contact force model would better reflect the relationship between the inter-particle force and the deformation, as proven by experimental and numerical results [13, 14]. Currently, the nonlinear Hertz–Mindlin contact force model has been widely adopted in the DEM simulation of granular materials. And the nonlinear normal viscous force model has been improved and verified by experiments [15]. However, the normal viscous force has not been well combined with the Hertz–Mindlin model. As for the tangential viscous force, there are some nonlinear models developed, but they have not been verified by experiments. Moreover, the tangential viscous force has little effect on the dynamics of granular materials and is often ignored in the DEM simulation [16].

Therefore, the objective of this paper is to develop a succinct 3D DEM model with clumps to resemble the real irregular shapes of granular materials. A finite partition approach is first used to calculate the mass, center of mass and moment of inertia of a clump in the local coordinates. The rotation, the resultant force and moment acting on a clump are then calculated both in the global and local coordinates, and the quaternion method is introduced to obtain the transformation matrix between coordinates. The Hertz–Mindlin elastic contact force model, with the incorporation of the nonlinear normal viscous force and the Mohr–Coulomb friction law, is used to describe the interactions between particles. Based on the established DEM model, the direct shear tests of the irregular limestone rubbles are simulated. The numerical and measured results of the vertical displacements and shear stresses are compared.

DOI: 10.1002/nag

2. DISCRETE ELEMENT MODEL WITH CLUMPS

2.1. Mass and moment of inertia of a clump

A clump is discretized into finite cubes with dimension of $\Delta V = \Delta x \times \Delta y \times \Delta z$. For any arbitrary cube, only when it is inside a sphere, its contribution to the clump will be taken into account. Therefore, the mass, center of mass and moment of inertia of a clump in the local coordinates are determined as follows:

$$\tilde{M} = \rho \sum_{k=1}^{K} \Delta V_k \tag{1}$$

$$\tilde{X}_i = \frac{\rho \sum_{k=1}^{K} x_k \Delta V_k}{\tilde{M}} \tag{2}$$

$$\tilde{I}_{ii} = \rho \sum_{k=1}^{K} [(\tilde{X}_j - x_{kj})^2 \Delta V_k] \tag{3}$$

where $\tilde{M}$, $\tilde{X}_i$ and $\tilde{I}_{ii}$ are the estimated mass, center of mass and local moment of inertia of the clump. ρ is the particle density and K is the effective number of cubes. ΔV_k and x_k are the volume and center of mass of cube k. The accuracy of the above estimation largely depends on the size of the discretized cube. Our results show that when $\Delta x = \Delta y = \Delta z = D_{\min}/20$ is set, where $D_{\min}$ is the minimum diameter of clumps, the calculations are close to their real values with an accuracy of 97%.

2.2. Motion of clumps using the quaternion method

For a clump, the global coordinates $\mathbf{e}^{\mathrm{G}}$ and the local coordinates $\mathbf{e}^{\mathrm{B}}$ are defined. The origin of the local one is located at the center of the clump as shown in Figure 1. The relationship of the local and global coordinates is written as,

$$\mathbf{e}^{\mathrm{B}} = \boldsymbol{A} \cdot \mathbf{e}^{\mathrm{G}} \tag{4}$$

$$\mathbf{e}^{\mathrm{G}} = \boldsymbol{A}^{\mathrm{T}} \cdot \mathbf{e}^{\mathrm{B}} \tag{5}$$

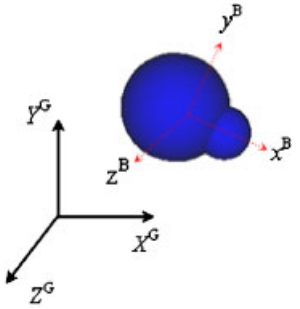

Figure 1. Local and global coordinates in the DEM simulation of clumps.

DOI: 10.1002/nag

where the transformation matrix $\boldsymbol{A}$ satisfies $\boldsymbol{A}^{-1}=\boldsymbol{A}^{\mathrm{T}}$ and can be determined by the quaternion method. There are four scalars in the quaternion method, that is [17],

$$\boldsymbol{Q}=(q_0, q_1, q_2, q_3) \tag{6}$$

with the property of

$$q_0^2+q_1^2+q_2^2+q_3^2=1 \tag{7}$$

Thus, the transformation matrix can be rewritten as [17]

$$\boldsymbol{A}=\begin{pmatrix} q_0^2+q_1^2-q_2^2-q_3^2 & 2(q_1q_2+q_0q_3) & 2(q_1q_3-q_0q_2) \\ 2(q_1q_2-q_0q_3) & q_0^2-q_1^2+q_2^2-q_3^2 & 2(q_2q_3+q_0q_1) \\ 2(q_1q_3+q_0q_2) & 2(q_2q_3-q_0q_1) & q_0^2-q_1^2-q_2^2+q_3^2 \end{pmatrix} \tag{8}$$

The moment components in the local coordinates can be obtained through the transformation of those in the global coordinates, that is,

$$\begin{pmatrix} M_x^{\mathrm{B}} \\ M_y^{\mathrm{B}} \\ M_z^{\mathrm{B}} \end{pmatrix}=\boldsymbol{A}\begin{pmatrix} M_x^{\mathrm{G}} \\ M_y^{\mathrm{G}} \\ M_z^{\mathrm{G}} \end{pmatrix} \tag{9}$$

where M_x^{B}, M_y^{B} and M_z^{B} are the moment components in the local coordinates. M_x^{G}, M_y^{G} and M_z^{G} are the moment components in the global coordinates and can be calculated through the contact force in the DEM simulation.

In the local coordinates, the rotational acceleration of a clump can be determined by [18]

$$\dot{\omega}_x^{\mathrm{B}}=\frac{M_x^{\mathrm{B}}}{\tilde{I}_{xx}}+\left(\frac{\tilde{I}_{yy}-\tilde{I}_{zz}}{\tilde{I}_{zz}}\right)\omega_y^{\mathrm{B}}\omega_z^{\mathrm{B}} \tag{10}$$

$$\dot{\omega}_y^{\mathrm{B}}=\frac{M_y^{\mathrm{B}}}{\tilde{I}_{yy}}+\left(\frac{\tilde{I}_{zz}-\tilde{I}_{xx}}{\tilde{I}_{yy}}\right)\omega_z^{\mathrm{B}}\omega_x^{\mathrm{B}} \tag{11}$$

$$\dot{\omega}_z^{\mathrm{B}}=\frac{M_z^{\mathrm{B}}}{\tilde{I}_{zz}}+\left(\frac{\tilde{I}_{xx}-\tilde{I}_{yy}}{\tilde{I}_{zz}}\right)\omega_x^{\mathrm{B}}\omega_y^{\mathrm{B}} \tag{12}$$

where ω_x^{B}, ω_y^{B} and ω_z^{B}, $\dot{\omega}_x^{\mathrm{B}}$, $\dot{\omega}_y^{\mathrm{B}}$ and $\dot{\omega}_z^{\mathrm{B}}$ are rotational velocities and accelerations of the clump in the local coordinates, respectively.

The quaternion components and the rotational velocities of the clump satisfy the following equation [18]:

$$\begin{pmatrix} \dot{q}_0 \\ \dot{q}_1 \\ \dot{q}_2 \\ \dot{q}_3 \end{pmatrix}=\frac{1}{2}\mathbf{W}\begin{pmatrix} 0 \\ \omega_x^{\mathrm{B}} \\ \omega_y^{\mathrm{B}} \\ \omega_z^{\mathrm{B}} \end{pmatrix} \tag{13}$$

DOI: 10.1002/nag

with

$$\mathbf{W}=\begin{pmatrix} q_0 & -q_1 & -q_2 & -q_3 \\ q_1 & q_0 & -q_3 & q_2 \\ q_2 & q_3 & q_0 & -q_1 \\ q_3 & -q_2 & q_1 & q_0 \end{pmatrix} \tag{14}$$

After the calculation of the local rotational velocities, the global rotational velocities can then be obtained:

$$\begin{pmatrix} \omega_x^{\mathrm{G}} \\ \omega_y^{\mathrm{G}} \\ \omega_z^{\mathrm{G}} \end{pmatrix} = \mathbf{A}^{\mathrm{T}} \begin{pmatrix} \omega_x^{\mathrm{B}} \\ \omega_y^{\mathrm{B}} \\ \omega_z^{\mathrm{B}} \end{pmatrix} \tag{15}$$

With the above transformation between local and global coordinates using the quaternion method, the equations of motion are integrated using the explicit differential scheme involving a time step of Δt.

Initially, the positions and orientations of particles are given in global coordinates and global Euler angles, and the quaternion has the relationship with Euler angles as follows:

$$\begin{aligned} q_0^{(0)} &= \cos\frac{\theta}{2}\cos\frac{\phi+\psi}{2} \\ q_1^{(0)} &= \sin\frac{\theta}{2}\cos\frac{\phi-\psi}{2} \\ q_2^{(0)} &= \sin\frac{\theta}{2}\sin\frac{\phi-\psi}{2} \\ q_3^{(0)} &= \cos\frac{\theta}{2}\sin\frac{\phi+\psi}{2} \end{aligned} \tag{16}$$

where θ, ϕ and ψ are the Euler angles. The transformation matrix $\mathbf{A}^{(0)}$ is determined with Equation (8). The translational velocity and rotational velocity of each clump are given randomly in global coordinates.

At time $n\Delta t$, the resultant force and moment acting on a clump are $(\mathbf{F}_G^{(n)}, \mathbf{M}_G^{(n)})$ in global coordinates, and the moment in local coordinates can be transformed from global coordinates by Equation (9).

At time $(n+1)\Delta t$, the translational velocity can be calculated as

$$\mathbf{V}_G^{(n+1)} = \mathbf{V}_G^{(n)} + \frac{\mathbf{F}_G^{(n)}\Delta t}{\tilde{M}} \tag{17}$$

where $\mathbf{V}_G^{(n+1)}$ and $\mathbf{V}_G^{(n)}$ are the translational velocity of a clump in global coordinates at time $n\Delta t$ and $(n+1)\Delta t$, respectively.

DOI: 10.1002/nag

The rotational velocity at time $(n+1)\Delta t$ in local coordinates can be calculated using Equations (10)–(12). The quaternions at $(n+1)\Delta t$ can be determined with Equation (13) by

$$\begin{pmatrix} q_0 \\ q_1 \\ q_2 \\ q_3 \end{pmatrix}^{(n+1)} = \begin{pmatrix} q_0 \\ q_1 \\ q_2 \\ q_3 \end{pmatrix}^{(n)} + \frac{\Delta t}{2}\mathbf{W}^{(n)} \begin{pmatrix} 0 \\ \omega_x^{\mathrm{B}} \\ \omega_y^{\mathrm{B}} \\ \omega_z^{\mathrm{B}} \end{pmatrix}^{(n)} \tag{18}$$

The transformation matrix $\mathbf{A}^{(n+1)}$ at time $(n+1)\Delta t$ can be calculated with Equation (8), and the rotational velocity of each clump in global coordinates can be updated by

$$\begin{pmatrix} \omega_x^{\mathrm{G}} \\ \omega_y^{\mathrm{G}} \\ \omega_z^{\mathrm{G}} \end{pmatrix}^{(n+1)} = \mathbf{A}^{(n+1)^{\mathrm{T}}} \begin{pmatrix} \omega_x^{\mathrm{B}} \\ \omega_y^{\mathrm{B}} \\ \omega_z^{\mathrm{B}} \end{pmatrix}^{(n+1)} \tag{19}$$

With the translational velocity and rotational velocity in global coordinates obtained with Equations (17) and (19), the contact force and moment at time $(n+1)\Delta t$ may be calculated.

2.3. Nonlinear contact force model

The contacts between clumps and a clump and a sphere are contacts of two regular spheres. Thus, the contact force model of two spheres is used to calculate the contact force between particles. In the normal direction, the contact force consists of elastic and viscous forces. Based on Hertz's theory of the particle–particle contact of two elastic spheres, the normal contact force can be written as [19]

$$F_{\mathrm{n}} = K_{\mathrm{n}} x_{\mathrm{n}}^{3/2} + \tfrac{3}{2} A K_{\mathrm{n}} x_{\mathrm{n}}^{1/2} \dot{x}_{\mathrm{n}} \tag{20}$$

Without considering the viscous force in the tangential direction, and with the consideration of the Mohr–Coulomb friction law, the shear force can be determined as [20]

$$F_{\mathrm{s}}^{*} = K_{\mathrm{s}} x_{\mathrm{n}}^{1/2} x_{\mathrm{s}} \tag{21}$$

$$F_{\mathrm{s}} = \min(F_{\mathrm{s}}^{*}, \mathrm{sign}(F_{\mathrm{s}}^{*})\mu F_{\mathrm{n}}) \tag{22}$$

where x_{n} and $\dot{x}_{\mathrm{n}}$ are the normal deformation and deformation rate, respectively. x_{s} is the shear deformation and μ is the friction coefficient. A is a material constant depending on Young's modulus, viscous coefficients and Poisson ratio of the material and can be determined by the restitution coefficient of particle collisions at a certain speed [19]. K_{n} and K_{s} in the above contact model can be calculated as [20]

$$K_{\mathrm{n}} = \tfrac{4}{3} E^{*} \sqrt{R^{*}} \tag{23}$$

$$K_{\mathrm{s}} = 8 G^{*} \sqrt{R^{*}} \tag{24}$$

DOI: 10.1002/nag

where

$$E^*=\frac{E}{2(1-\upsilon^2)},\quad G^*=\frac{G}{2(2-\upsilon)},\quad G=\frac{E}{2(1+\upsilon)},\quad R^*=\frac{R_AR_B}{R_A+R_B}$$

E,υ and G are Young's modulus, Poisson ratio and shear modulus of the material. R_A and R_B are the radius of two particles in contact.

The maximum time step in the nonlinear DEM can be determined by [21]

$$t_{\max}=\frac{\pi R_{\min}}{0.163\upsilon+0.8766}\sqrt{\frac{\rho}{G}} \tag{25}$$

The real time step in the calculation is less than the maximum, and is determined by

$$dt=\alpha t_{\max} \tag{26}$$

where α is an empirical coefficient. Normally, with higher coordination number (>4), a smaller time step is set as $dt=0.2t_{\max}$, and with lower coordination number (<4), $dt=0.4t_{\max}$ [21]. In this study, we set $\alpha=0.2$.

3. SIMULATION OF DIRECT SHEAR TESTS FOR IRREGULAR LIMESTONE RUBBLES WITH THE PROPOSED DEM

3.1. Laboratory direct shear tests

The direct shear box includes an upper and lower box. The initial gap between the two boxes is normally set as half of the mean particle diameter. Vertical loads are applied at the top wall of the upper box and the lower box is sheared horizontally with a constant shear rate. In addition, the upper box is fixed horizontally and free to move vertically, while the lower box fixed vertically and free to move horizontally. The vertical displacement and shear stress were measured under three different normal stresses (100, 200 and 300 kPa).

The mass of 300 particles of limestone rubbles, randomly selected from the specimen, were measured and found to obey a lognormal distribution,

$$f(m)=\frac{1}{m\sigma\sqrt{2\pi}}\exp\left(-\frac{1}{2}\left(\frac{\ln m-\mu}{\sigma}\right)^2\right) \tag{27}$$

with the probability distribution parameters $\sigma=0.432$ and $\mu=-0.117$. Figure 2 shows the measured and fitted probability density distribution of the tested material, and Table I lists the mechanical properties of the physical material.

3.2. DEM modeling of direct shear tests with clumps

To model the real irregular shapes of the limestone rubbles, four different clumps were constructed as shown in Figure 3. Overlapping size of any two spheres was randomly distributed in the range of $[0.0, 0.5D_{\min}]$. In Figure 3(a), (c) and (d), spheres have the same diameters, while in Figure 3(b), the diameter of the larger sphere is two times that of the smaller one. The sizes of clumps were determined by their mass, which in turn can be generated by Monte Carlo method based on the measured lognormal distribution of the mass of the specimen as shown in Figure 2.

DOI: 10.1002/nag

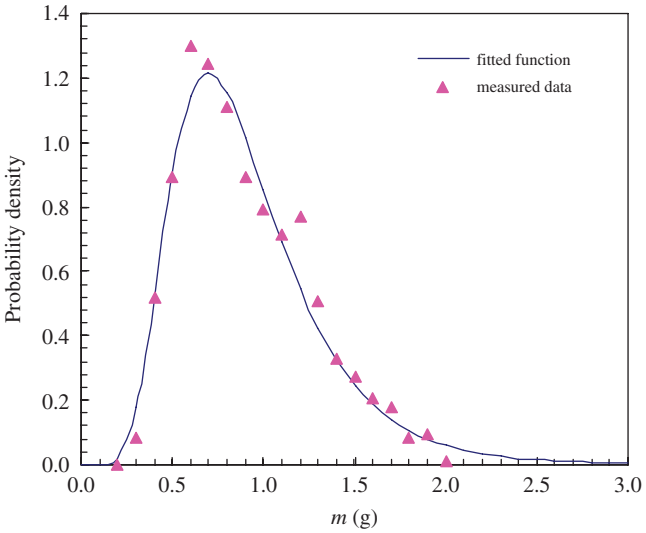

Figure 2. The probability density distribution of the physical material.

Table I. Mechanical properties of the irregular limestone rubbles.

Parameter	Definition	Value
M	Total mass of the specimen	973.6 g
m	Mass of a single particle	0.4–2.0 g
D	Diameter of sphere	1.30–2.42 mm
ρ	Density	2.545×10^3 kg/m^3
E	Young's modulus	58.54 GPa
υ	Poisson ratio	0.221

If spheres were used here instead, it would be hard to simulate the interlocking between particles, even for the sand, which has rather simple and regular geometry. Although in this case the contact friction coefficient could be increased to improve the macroshear characteristics, simulations showed the results are acceptable when the contact friction coefficient is set as 60 or 80, which far exceeds its real value [22]. Our study tries to use a mixture of clumps presented above to realize the interlocking between particles so that the shear behavior can be better modeled.

In the DEM simulation, particles were placed randomly in the box. To produce a compacted assembly initially, the particle size was set as half of its real value, and particles were allowed to grow slowly until the required size was reached. This radius-expansion scheme is commonly used in the DEM simulation of granular materials. The external vertical load was then applied on the top wall of the upper box to obtain an initial equilibrium state. The box was finally sheared with a given shear rate of U until the critical state was reached. The major parameters used in the DEM simulation are listed in Table II.

Figure 4 shows the DEM model of the test with clumps resembling the irregular limestone rubbles. Different colors are used to distinguish different particles.

DOI: 10.1002/nag

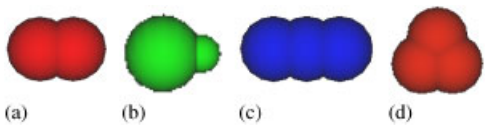

Figure 3. Clumps used in the DEM simulation.

Table II. Parameters used in the DEM simulation.

Variables	Definition	Values
L	Length of the shear box	10 cm
B	Width of the shear box	10 cm
H_1, H_2	Height of the upper and lower box	3.71 cm
μ_p	Friction coefficient between particles	0.7
μ_{ws}	Friction coefficient between particles and side walls of the shear box	0.2
μ_{wb}	Friction coefficient between particles and the top/bottom wall of the shear box	1.0
U	Shear rate in the test	3.0 mm/min
N_p	Number of spheres	2300
N_c	Number of clumps	926

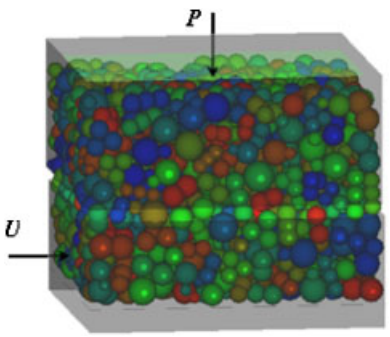

Figure 4. The DEM model of the direct shear test with clumps resembling the limestone rubbles.

The normal force acting on the shear band is the sum of the weight of the upper box W_B, the weight of particles inside W_P and the external load P. And the shear force can be determined through the equilibrium in the horizontal direction. Therefore, the normal force F_N and the shear force F_S acting on the shear band can be calculated as follows:

$$F_N = P + W_P + W_B \tag{28}$$

$$F_S = \sum_{iw=1}^{N_{wall}} (N_{X_{iw}} + S_{X_{iw}}) \tag{29}$$

DOI: 10.1002/nag

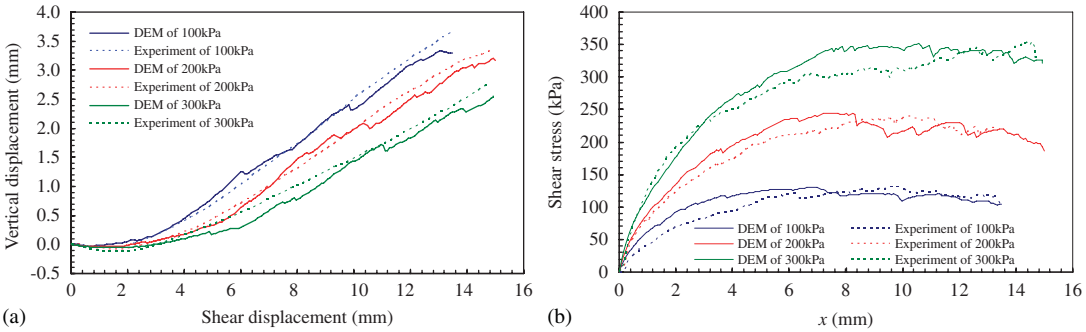

Figure 5. Simulated and measured vertical displacements (a) and shear stresses (b) under three different normal stresses (100, 200 and 300 kPa).

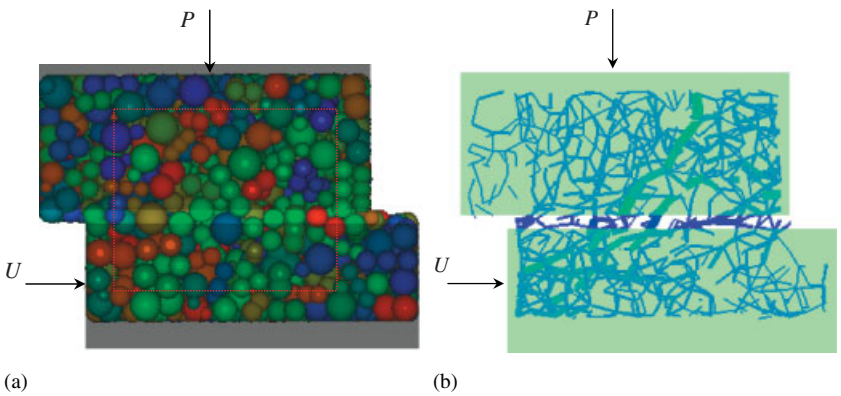

Figure 6. Particle system (a) and distribution of the force (b) in the critical state of shearing.

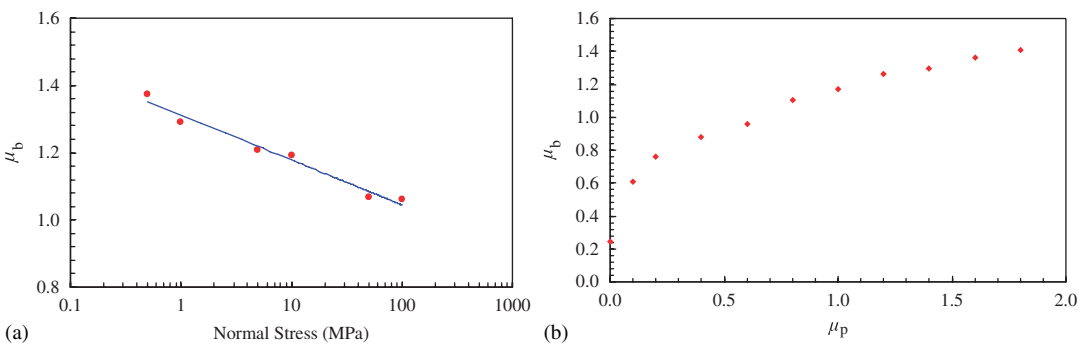

Figure 7. Simulated bulk friction coefficients under different normal stresses (a) and contact frictions (b).

DOI: 10.1002/nag

where $N_{X_{iw}}$ is the normal force acting on the left and right side wall of the upper box by inside particles, and $S_{X_{iw}}$ is the shear force acting on the upper box. The upper box has four side walls and a top, and the total wall number $N_{\text{wall}}=5$.

The length and width of the shear box are L and B. The box was sheared with a shear rate of U. At any time t, the area of the shear band is $B(L-Ut)$. The normal and shear stress in the shear band can be obtained as

$$\sigma_{zz}=\frac{F_{\text{N}}}{B(L-Ut)} \tag{30}$$

$$\tau_{zx}=\frac{F_{\text{S}}}{B(L-Ut)} \tag{31}$$

where σ_{zz} and τ_{zx} are the normal and shear stress in the shear band. And the bulk friction coefficient is calculated as

$$\mu_{\text{b}}=\frac{\tau_{zx}}{\sigma_{zz}}=\frac{F_{\text{S}}}{F_{\text{N}}} \tag{32}$$

3.3. Results of laboratory tests and proposed DEM simulations

The vertical displacement z and the shear stress τ_{zx} of the laboratory tests and the DEM simulations are plotted in Figure 5, and they are quite close. Figure 5(a) clearly shows the dilatancy with the increase of the shear displacement. In particular, under small normal stress, dilatancy is remarkable. In addition, there exists a downward displacement at the initial period of shearing, that is, the specimen experienced a contraction. This contraction is usually small (<2 mm) and increases with the increase of the normal stress. This phenomenon indicates the coexistence of rotation and sliding in sheared granular materials, especially near the shear band. At the beginning of shearing, the rotation results in a compacted particle system. As the shear displacement increases, the rotation leads to extensive dilatancy. The contraction-dilatancy is one of the typical characteristics of granular materials, and has been verified in direct shear tests of other materials [23].

Figure 6 shows the particle system and transmission of the force inside the box in the critical state of shearing. In Figure 6(b), lines are drawn between centers of two particles in contact and the width of lines represents the amplitude of the contact force. It clearly shows that the distribution of contact force is not uniform, and the shear and normal stress are supported mainly along the direction of the diagonal going from upper right to lower left of the box. This anisotropy of direct shear tests has been found both in DEM simulation and laboratory tests [3, 24].

With different normal stresses σ_{zz} and contact friction coefficients μ_{p} between particles, the bulk friction coefficient μ_{b} was calculated with the established DEM model. Figure 7 gives the simulation results. It shows in Figure 7(a) the bulk friction coefficient decreases with the increase of the normal stress. This can be explained by Mohr envelope of the shear strength of granular materials. Figure 7(b) shows that the bulk friction coefficient increases as the contact friction coefficient μ_{p} increases, but with a decreasing increase rate. This is mainly because rotation and sliding both occur in the shearing process, and the increase of the contact friction coefficient further stimulates the rolling effect of particles. Currently, studies on the competition mechanism between sliding friction and rolling resistance are important in improving the accuracy of numerical simulations of granular dynamics.

DOI: 10.1002/nag

4. CONCLUSIONS

Direct shear tests of the irregular limestone rubbles were simulated by 3D DEM with a mixture of clumps resembling the real shapes of the material. Clumps were constructed by overlapping spheres with different numbers, diameters, orientations and overlapping lengths, and provided the interlocking among particles. The characteristics of direct shear of irregular granular materials can be modeled well with the developed clumps. The simulation results agreed well with that of laboratory tests. The simulations also showed that the bulk friction coefficient increases with the increase of the contact friction coefficient and increases with the decrease of the normal stress. In addition, the introduction of the quaternion method resulted in relatively simple calculations.

ACKNOWLEDGEMENTS

The authors were grateful to Prof. Hayley H. Shen from Department of Civil and Environmental Engineering, Clarkson University, U.S.A., for her helpful discussions and Mr Xinbao Yu from the same university for his assistance on direct shear tests. This work was sponsored by the National Natural Science Foundation of China 10772041, 50808027, and the Scientific Research Foundation for the Returned Overseas Scholars, State Education Ministry 2008-890.

REFERENCES

1. Tejchman J. FE analysis of shearing of granular bodies in a direct shear box. *Particulate Science and Technology* 2005; **23**:229–248.
2. Cividini A, Gioda G. A finite element analysis of direct shear tests on stiff clays. *International Journal for Numerical and Analytical Methods in Geomechanics* 1992; **16**:869–886.
3. Thornton C, Zhang L. Numerical simulation of the direct shear test. *Chemical Engineering and Technology* 2003; **26**(2):153–156.
4. Liu SH. Simulating a direct shear box test by DEM. *Canadian Geotechnical Journal* 2006; **43**:155–168.
5. Cleary PW, Sawley ML. DEM modelling of industrial granular flows: 3D case studies and the effect of particle shape on Hopper discharge. *Applied Mathematical Modelling* 2002; **26**:89–111.
6. Ting JM, Khwaja M, Meachum L *et al.* An ellipse-based discrete element model for granular materials. *International Journal for Numerical and Analytical Methods in Geomechanics* 1993; **17**:603–623.
7. Cheng YP, Nakata Y, Bolton MD. Discrete element simulation of crushable soil. *Geotechnique* 2003; **53**(7): 633–641.
8. Jensen RP, Josscher PJ, Plesha ME, Edil TB. DEM simulation of granular media–structure interface: effect of surface roughness and particle shape. *International Journal for Numerical and Analytical Methods in Geomechanics* 1999; **23**:531–547.
9. Itasca Consulting Group Inc. *Online Manual of Particle Flow Code in 3 Dimensions* (*PFC*^{3D}) *Version 3.0.* Itasca: Minneapolis, 2003.
10. Lim WL, McDowell GR. Discrete element modeling of railway ballast. *Granular Matter* 2005; **7**:19–29.
11. Peters B, Dziugys A. Numerical simulation of the motion of granular material using object-oriented techniques. *Computer Methods in Applied Mechanics and Engineering* 2002; **191**:1983–2007.
12. Smith R, Frost A, Probert PJ. Gyroscopic data fusion via a quaternion-based complementary filter. Sensor fusion: architectures, algorithms, and applications. *Proceedings of the SPIE* 1997; **3067**:148–159.
13. Ji S, Shen H. Effect of contact force models on granular flow dynamics. *ASCE Journal of Engineering Mechanics* 2006; **132**(9):1252–1259.
14. Mishra BK, Murty CVR. On the determination of contact parameters for realistic DEM simulations of ball mills. *Powder Technology* 2001; **115**:290–297.
15. Schager T, Poschel T. Coefficient of restitution of viscous particles and cooling rate of granular gases. *Physical Review E* 1998; **57**(1):650–654.
16. Campbell C. Granular shear flows at the elastic limit. *Journal of Fluid Mechanics* 2002; **465**:261–291.

DOI: 10.1002/nag

17. Fritzer HP. Molecular symmetry with quarternions. *Spectrochimica Acta Part A* 2001; **57**:1919–1930.
18. Allen MP, Tildesley DJ. *Computer Simulation of Liquids*. Oxford University Press: London, 1987; 30–90.
19. Ramirez R, Poschel T, Brilliantov NV *et al.* Coefficient of restitution of colliding visco-elastic sphere. *Physical Review E* 1999; **60**(4):4465–4472.
20. Di Renzo A, Di Maio FP. An improved integral non-linear model for the contact of particles in distinct element simulations. *Chemical Engineering Science* 2005; **60**:1303–1312.
21. Kremmer M, Favier JF. A method for representing boundaries in discrete element modelling—Part II: kinematics. *International Journal for Numerical Methods in Engineering* 2001; **51**:1423–1436.
22. Zhou J, Chi Y. Simulation soil properties by particle flow code. *Acta Mechanica Solida Sinica* 2004; **25**(4): 377–382.
23. Dittes M, Labuz JF. Field and laboratory testing of St. Peter Sandstone. *Journal of Geotechnical and Geoenvironmental Engineering* 2002; **128**(5):372–380.
24. Fannin RJ, Eliadorani A, Wilkinson MT. Shear strength of cohesionless soils at low stress. *Geotechnique* 2005; **55**(6):467–478.

DOI: 10.1002/nag